Design of a Smart Tether Winch for an Autonomous ROV/USV System

Charly Peraud, David Eskoundos, Cédric Anthierens, Vincent Hugel

Design of a Smart Tether Winch for an Autonomous ROV/USV System

Charly PERAUD[a], David ESKOUNDOS[a], Cédric ANTHIERENS[a], Vincent HUGEL[a]

[a] *COSMER Laboratory, University of Toulon, France*

Abstract

Although ROVs are highly effective for shallow-water missions, the umbilical remains a source of hazard. When combined with a USV, the ROV benefits from a significantly extended workspace. However, the trajectory of the USV is generally controlled manually, and the dynamic behavior of the umbilical cable remains unmanaged. This paper introduces a distributed mechatronic solution between the ROV and the USV that enables continuous and on-demand control of the umbilical to facilitate effective cooperation between the two robots. The solution consists of a two-part system: a compliant V-shape sensor mounted on the umbilical just aft of the ROV, and an intelligent winch that dynamically regulates the umbilical length. This innovative design enables automatic and coordinated control of the ROV / USV system, which has been validated by experiments in water tanks.

Keywords: Sensorimotor interface, ROS, marine sensors, cable behavior.

1. Introduction

Underwater missions led by robotics systems are numerous and very different in needs depending on their duration, range, depth and also their goals that can be civil, industrial or military purposes [1, 2]. To meet these various requirements, unmanned underwater vehicles can be sorted in three main types which are the AUV (Autonomous Underwater Vehicle), UG (Underwater Glider) and ROV (Remotely Operated Vehicle) [3, 4]. Although these robots feature great interests related to the safety and the ease to be deployed, only ROVs rely on a cable linked to the surface for power supply or at least, for real-time communication and control. To extend their

operational range, ROVs are commonly assisted by a surface mobile base station, which can be a vessel, or more recently a USV (Unmanned Surface Vehicle) [5, 6]. Then both robots of the coupled ROV/USV system can work together to achieve long missions in duration and range by being remotely controlled from a long range ground station. Such a system is particularly well-suited for random exploration, environmental monitoring, and surveying features in shallow water [7]. Priority is given to coastal areas near the shoreline, where wave activity generates water currents and the seabed is often partially covered by marine vegetation, such as "Posidonia" in the Mediterranean Sea. Moreover, the presence of underwater rocks and cliffs, which are common in shallow environments, may require dynamic three-dimensional navigation by the ROV [8].

1.1. Needs

Such environmental characteristics give rise to mission-specific requirements, which may include random exploration, the search for points of interest, or area coverage tasks. Exploring wide areas that may be far from each other actually requires to deal with a long tether, that may generate many troubles like hampering ROV motion due to high drag forces increasing with the motion of robots or the water current, or entanglements against underwater obstacles or the tether itself [9].

Moreover, obtaining the 3D localization of the ROV relative to the USV frame is challenging, as systems such as Ultra-Short Baseline (USBL) may not always be available or sufficiently accurate in shallow water environments. In this context, the USV requires reliable data in order to accurately follow the ROV throughout the mission [10, 11]. Considering these physical and functional characteristics, it is essential to design a solution that equips the ROV / USV system with the ability to automatically manage the tether, like maritime winch, not only to mitigate its drawbacks but also to leverage its potential for enabling new localization functionalities.

2. Related Works

2.1. State of the Art of Maritime Winches

Few studies have explored advanced modeling and control strategies for coupled USV / underwater vehicle / winch systems, without having progressed beyond laboratory environments. Zhao et al. [12, 13] conducted detailed analytical and hydrodynamic simulations of winch performance

and ROV launch/recovery procedures. However, their work remains purely simulation-based and does not include any real-world implementation of automated tension control or cable's exit angle feedback. Similarly, Gu et al. [14] proposed a deep reinforcement learning (DRL)-based coordination scheme between a buoy and a winch, but this too was only validated in simulation. Earlier efforts by Moh et al. [15], who developed a wave-powered winch-towed acoustic sensor for USVs, and Bye et al. [16], who introduced an AI-based winch prototyping framework, also lack practical deployment features such as continuous tension regulation or directional cable sensing.

To date, only two research teams have proposed tethered USV / underwater vehicle systems with partial autonomy. Cho *et al.* [5] developed a catamaran-type USV with a tethered unmanned underwater vehicle for real-time data transmission and waypoint tracking, but the winch remains manually operated without active tension or cable-length control. As a result, the tether alternates between fully slack and fully taut configurations, which increases the risk of drag and entanglement in dynamic aquatic conditions. Kapetanović *et al.* [7] introduced a Tether Management System (TMS) with cable length control using USBL-based localization. Their solution is effective but relies on a safety buffer in the tether length due to slow-rate localization feedback, which limits the system's responsiveness and can still result in risky configurations during the mission.

2.2. Remaining Gaps

While both approaches demonstrate the feasibility of a cable-linked USV / underwater vehicle system with real-time communication and coordinated navigation, key challenges remain unaddressed:

- **Automated tension control:** Neither system provides continuous and on-request regulation of tether tension to minimize drag or prevent entanglement during vehicle motion.
- **Directional cable feedback:** No solution offers direct sensing of the cable's exit angle from the surface vehicle, which would enable passive heading alignment or active steering.
- **Low-cost localization:** Both rely on expensive USBL; However, it is possible to integrate more affordable onboard methods (e.g. inertial or mechanical cable-based).

- **Slack management without large buffers:** The Croatian [7] TMS's 3 m buffer reduces dynamic tension but leaves substantial cable loose; a tighter, self-adjusting slack regime is needed for safer operations in cluttered environments.

2.3. Proposed Solution

The solution proposed in this work aims to fill these gaps and consists of a two-part system integrated along the tether connecting a mission-performing ROV to its follower USV. Its primary function is to automatically adjust cable length between the two robots to ensure that the ROV keeps full maneuverability, while simultaneously minimizing risks associated with an excessively slack or overly taut tether. A secondary function of the system is to provide continuous data about the cable's behavior, particularly regarding its position relative to both robots. Hence, such information would help the USV to follow the ROV by favoring some chosen criteria (distance, energy consumption, localization accuracy...).

The first part of the system is a compliant and sensorized structure installed along the tether near the ROV (see Section 3). Its role is to act as a mechanical damper and to sense situations where the tether becomes too slack or too taut. The second part is a smart winch mounted on the USV, which uses the sensory feedback from the compliant device to actively reel in or release the tether on demand (see Section 4). Additionally, the winch is equipped with microswitch sensors that detect the direction in which the tether departs relative to the USV frame in order get information about its behavior.

This paper is organized as follows. Section 3 and Section 4 introduce the mechatronical design of the proposed solution. Section 5 presents the Human-Machine Interface developed to monitor and operate the complete system. Section 6 outlines the experiments conducted to validate the proper working of the system and to discuss the results. Finally Section 7 concludes the paper and presents future research prospects.

3. V-shape System Design

The compliant V-shape system developed in this work is based on the solution proposed in prior studies [17, 18]. A 50-meter-long neutrally buoyant umbilical, made of a 4 mm diameter twisted pair and wound on the winch, ensures communication between the ROV and the USV. The V-shape system

is positioned along the umbilical about 10 cm behind the ROV and consists of two buoys spaced 120 cm apart, with a ballast positioned precisely between them, designed to form a balanced "V-shape" at rest — hence the name (Fig. 1). The ballast has a mass of approximately 75 g and each buoy consists of a foam cuboid element with a volume of 39 cm^3 a density of 288 $kg.m^{-3}$. Both buoys and the ballast were designed to achieve neutral equilibrium underwater. In the original version, a flex sensor (specifically, a strain gauge) was integrated at the ballast, aiming to reflect the distance between the buoys. By analyzing this signal, it was possible to determine whether the cable became too slack or too taut, in which case the cable length had to be adjusted. This V-shape system serves several purposes:

- to passively reduce the forces exerted on the ROV when the tension increases in the cable,
- to detect the intention of movement on both sides of the V-shape system,
- to deliver the appropriate cable length, maintaining a so-called "semi-taut" configuration, thus helping to minimize drag forces and the risk of entanglement with the environment.

In practice, the waterproofing solution for the flex sensor has proven unsustainable over time, as the measurement relies on deformation, which tends to damage the sealing system. To address this issue, a previous work [11] studied the replacement of this sensor with several inertial measurement units (IMUs) distributed along the V-shape system. This study showed that the data provided by the IMUs allows an accurate estimation of the distance between the buoys, and can also provide insight into the behavior of the V-shape system, such as out-of-plane configuration, remaining compliance capacity, and relative orientation of the cable's ends.

This new version of the system uses two IMUs placed on the tether, and the ballast is clamped via a pendulum joint to allow it to hang vertically downward, ensuring that the V-shape remains within an almost vertical plane even when the ROV is turning. In addition, its balance in buoyancy keeps it almost horizontal behind the ROV since the tether is slack or semi-taut. Such a behavior is also maintained while the ROV is moving forward in any configuration relative to the USV. The next section presents the implementation of the IMUs on the new V-shape system and its behavior through experimentations in the air.

3.1. Integration of IMUs on the umbilical

The IMUs used in this study are the *BMX160*[1] modules from *DFRobot*. These sensors integrate a 3-axis accelerometer, a 3-axis gyrometer, and a 3-axis magnetometer, enabling full 9-axis motion sensing. Designed for low power consumption, each module operates at less than 1.5 mA under a 5 V supply. In terms of measurement capabilities, the accelerometer provides a configurable range from $\pm 2g$ to $\pm 16g$ with a resolution of 16 bits, allowing precise linear acceleration measurements. The gyrometer supports selectable ranges from $\pm 125°/s$ to $\pm 2000°/s$, also with a 16-bit resolution. The magnetometer offers measurement ranges of ± 1300 μT on the X and Y axes and up to ± 2500 μT on the Z axis, with a resolution of 13 bits. These sensors support both I^2C and SPI communication protocols.

This new instrumentation of the V-shape system uses two BMX160 modules positioned precisely on the cable between each buoy and the ballast (Fig. 1). Waterproofing was achieved using epoxy resin. Sensor data are acquired via the ROV's onboard Raspberry Pi 3B+ microcontroller using the I^2C protocol, at a sampling frequency of 25 Hz. This offers a balanced trade-off between system load and measurement quality suitable for control applications.

3.2. Estimation of Interbuoy Distance

The IMUs were positioned such that their local x-axis aligns with the direction of the cable and is oriented toward the ballast. In the absence of external disturbances acting on the cable, the acceleration measured by the i_{th} IMU, denoted as $a^i = \left(a^i_x, a^i_y, a^i_z\right)$, is solely due to the Earth's gravitational field. Under this condition, it is possible to estimate the inclination angle α^i of the IMU x-axis using Eq. 1. Assuming that the 0.6-meter-long segment of cable between a buoy and the ballast remains straight, the distance between the buoys, denoted as d_{BB} — also referred to as the interbuoy distance — can be estimated based on the inclination angles of the internal and external IMUs, denoted respectively by α^{int} and α^{ext}, using Eq. 2.

$$\alpha^i = \arccos \frac{a^i_x}{g} \tag{1}$$

$$d_{BB} = 0.6 \left(\sin \alpha^{int} + \sin \alpha^{ext}\right) \tag{2}$$

[1] `https://wiki.dfrobot.com/BMX160_9_Axis_Sensor_Module_SKU_SEN0373`

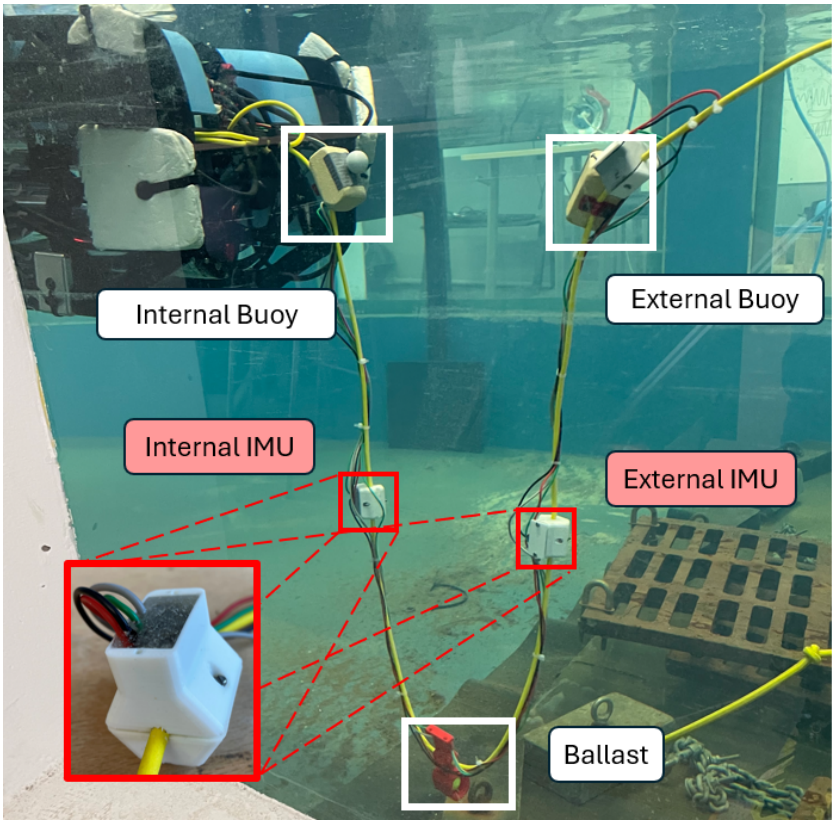

Figure 1: IMU-Based V-shape system on Umbilical

Several experiments were conducted to assess the accuracy of this estimation, as presented in Fig. 2. During the experiments, the buoys were placed at varying distances, and the interbuoy distance was estimated using Eq. 2. Due to the natural curvature of the cable near the ballast, the data become unreliable when the real distance is small (less than 0.3 m). As expected, the estimated distance converges toward the actual distance as the cable straightens. Based on these results, a second-order polynomial function was selected to fit the relationship between the estimated and actual distances in static.

4. Winch Design

The winch was designed to fulfill two main functions. The first is to deliver the tether on demand, in order to adapt to the motion of the ROV

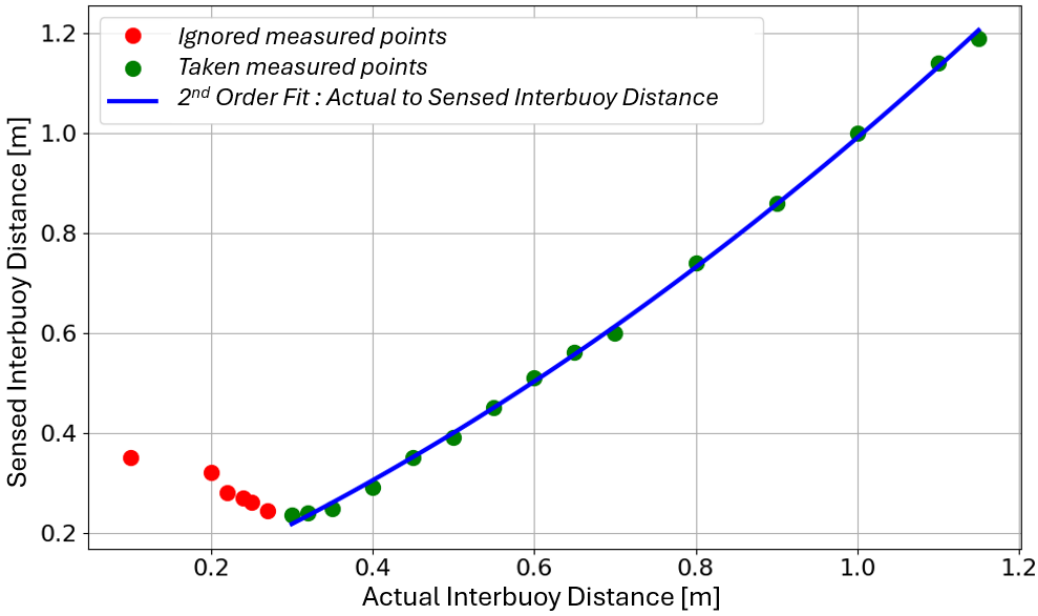

Figure 2: Sensed Interbuoy Distance vs Actual Interbuoy Distance

and/or the USV. To ensure safe and repeatable operations, the tether must be arranged in an orderly manner. The second function is to detect the direction in which the tether is leaving the winch, which can help to estimate the ROV's localization. The technical solutions developed to achieve these functions are detailed in this section.

4.1. Mechatronics Design

4.1.1. Tension Module and Spooler

To satisfy the first function, a coupled solution was developed (Fig. 3). The release and reeling-in operations of the tether are managed by a tension module that regulates the cable's speed. To store the unreleased portion of the tether, a spooler was designed, ensuring a smooth, compact, and orderly arrangement of the cable. This solution is mounted on the USV and enclosed in a yellow waterproof housing for safety. An inlet, measuring 20 cm in width and 4 cm in height, was drilled into the front panel of the housing to allow the tether to pass through. The tension module is placed close to this inlet whereas the spooler is in the back of the housing.

The tension module uses two 52 mm diameter toothed wheels to grip the tether between them, enabling controlled movement in both directions

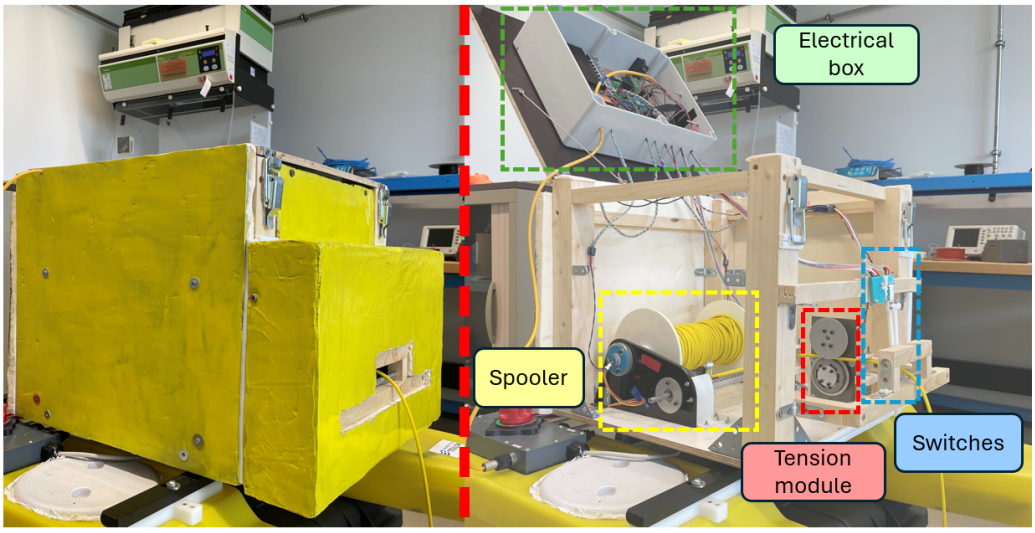

Figure 3: Overview of the winch with (left) and without housing (right)

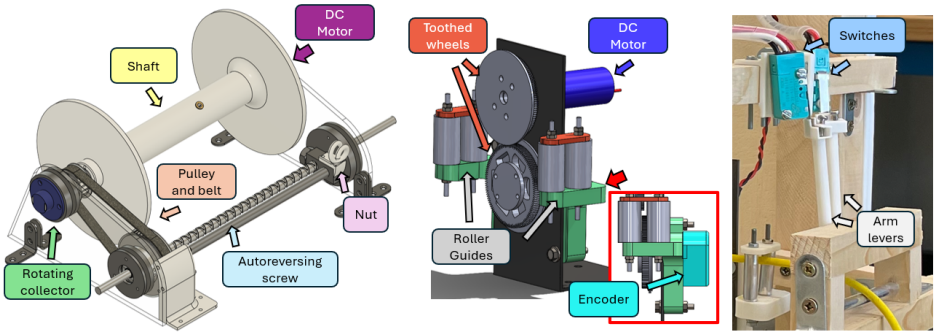

Figure 4: CAD representations of the Spooler (left) and Tension Module (middle), alongside the mounted microswitches (right).

through the housing (Fig. 4 middle). The upper wheel is actuated by a geared[2] DC motor[3]. The lower wheel is free, thus rotating only when the tether is passing, and is equipped with a 500 count/rev optical encoder that reachs a linear accuracy equal to 0.33 mm. Two roller-based guides are placed upstream and downstream of the tension module to keep the tether aligned with the two toothed wheels.

The spooler receives the tether from the tension module and is responsible for winding and arranging the coils (Fig. 4 left). It is composed of a shaft that is actuated from inside by a geared DC motor (same type as the tension module). An electrical rotating collector it placed at one of its ends to get the ROV data through the cable and transmit it to the USV motherboard. The rotating shaft drives an auto-reversing threaded screw via a pulley and belt system. A nut mounted on this screw slides back and forth, guiding the tether to ensure it is wound smoothly and evenly onto the shaft as it rotates in one direction. The pulleys were designed to achieve a linear shaft movement of 5 mm per step to wind the 4 mm diameter tether, preventing the coils from overlapping. This means the 20 cm long shaft can accommodate 40 coils of tether. Since the minimal radius of the winding is 17 mm, the first layer of coils represents 4,77 m of tether whereas the 10^{th} one about 9.29 m of tether. So a 70 m long tether is spooled in 10 layers of coils around a compact winding that is 74 mm in diameter. The way to control synchroniously the tension module and the spooler in both directions is addressed below in sections 4.1.3 and 4.2.

4.1.2. Switches

To obtain information about the shape and behavior of the tether, the housing is equipped with two microswitch sensors[4] that laterally guide the tether as it passes through the inlet (Fig. 4 right). Arm levers were added to enhance the sensors' sensitivity, allowing activation by the tether. Both sensors are positioned to maintain light contact with the tether and to be triggered when it deviates by approximately 20° from its initial orientation. However, since the tether is a flexible body, the sensors can only be triggered

[2] `https://www.maxongroup.com/medias/sys_master/root/8841509928990/FR-339.pdf`

[3] `https://www.maxongroup.com/medias/sys_master/root/8841231335454/FR-090.pdf`

[4] `https://fr.rs-online.com/web/p/microrupteurs/6990375`

if the tether is under tension. Therefore, only taut or semi-taut configurations are compatible with the correct operation of the sensors. These signals enable the detection of instances when the tether deviates to the right or left relative to the USV and can be integrated into autonomous control strategies.

4.1.3. Motor drivers

Although the geared DC motors of the tension module and the spooler are identical, they are controlled by two different electronic boards. Since the role of the tension module is to release a desired length of tether, a speed controller, fed by the optical encoder signal, is appropriate. This is achieved using the DC motor driver EM174A[5], which functions as a voltage amplifier and is actuated by the control law implemented on an Arduino Leonardo board.

The spooler, placed downstream of the tension module, must smoothly reel in the tether when it is pulled by the tension module. Although the speed and length of the tether are accurately known, the spooler cannot be easily controlled in speed or position due to the varying coil radius, which depends on the length of the wound tether. Moreover, a slightly taut portion of tether between the spooler and the tension module is required to ensure an orderly arrangement of the tether. For this purpose, torque control was implemented using the DC motor driver LSC 30/2[6], which supplies the motor with a current (and thus torque) proportional to the controller output computed on the Arduino board. This controller provides good performance for both releasing and reeling-in operations.

Although tether tension also depends on the winding radius, experiments showed that applying a constant torque value performs well across the entire range of radius variations in our setup. For longer tethers or alternative winch designs, different torque setpoints for the spooler may be required depending on the amount of tether wound on the reel.

4.2. Winch Behavior

4.2.1. Open-loop Command of Tension Module and Spooler

Several experiments were conducted to characterize the average natural behavior of the winch, taking into account the interaction between the

[5] https://docs.rs-online.com/a026/0900766b806b843e.pdf

[6] https://www.maxongroup.com/medias/sys_master/root/8834315354142/250521-LSC-30-2-Operating-Instructions-En.pdf

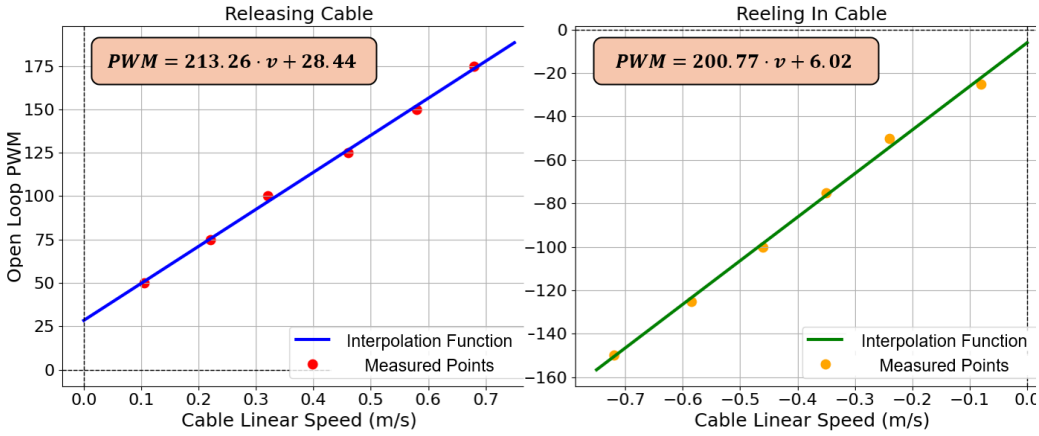

Figure 5: Open-loop Behavior of the Winch during Releasing (left) and Reeling (right) operations

tension module and the spooler during both cable releasing and reeling operations. In each case, the DC motor of the tension module was driven with various PWM inputs signals, while the resulting cable speed was measured using the encoder. Positive values of both the PWM input and the measured speed correspond to the cable release operation, whereas negative values indicate reeling. The spooler's DC motor was torque-controlled to compensate for resistive torque caused by mechanical static friction in the system. For the reeling operation, the desired torque applied to the spooler was experimentally tuned to maintain the cable straight between the spooler and the tension module, without exerting excessive pulling force. Conversely, during cable release, a smaller torque was applied to allow the cable to remain slightly slack, ensuring smooth unwinding. First-order polynomial models were fitted to the experimental data (Fig. 5) using the least squares method.

4.2.2. Speed Servoing of the Winch

To ensure that the winch delivers cable at the desired speed, a closed-loop speed control system (Fig. 6) was implemented on the DC motor of the tension module, using real-time speed measurements from the encoder. The variables with a superscript star denote desired values, such as the desired linear cable speed v^* or the desired angular speed of the geared motor ω^*. The parameters of the DC motor are presented in Tab. 1. As previously mentioned, the value of $C_{R_{eq}}$ is varying, depending on both the lateral position of the cable on the spooler (center vs. edges), the number of cable

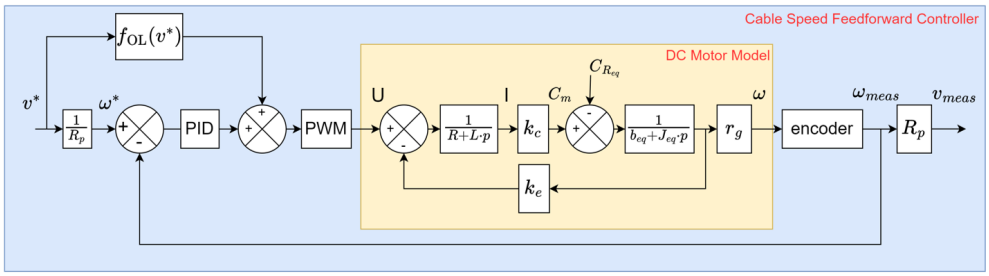

Figure 6: Closed-loop Speed Servoing Diagram for the DC motor of the Tension Module

layers already wound and also the pulling force exerted by the cable. The expressions of b_{eq} and J_{eq} are derived from the angular momentum theorem and are presented in Eq. 3 and Eq. 4.

$$b_{eq} = \frac{{r_g}^2}{\eta_g} b_p R_p \tag{3}$$

$$J_{eq} = J_m + \frac{{r_g}^2}{\eta_g} \left(J_g + 2\frac{m_p {R_p}^2}{2} \right) \tag{4}$$

A combination of feedforward and PID control was employed to regulate the motor's behavior. The feedforward controller aims to provide the DC motor with the input signal it would require in the absence of disturbances, while the PID controller compensates for deviations caused by unmodeled dynamics or external perturbations. The feedforward function f_{OL} is based on the average open-loop response of the winch, as characterized in Fig. 5. Since the winch exhibits distinct behaviors during releasing and reeling operations, separate PID gains were set experimentally for each operation mode.

An experiment was conducted to fine-tune the PID gains of the closed-loop speed control of the winch for both releasing and reeling operations (Fig. 7). Several speed step commands were applied during the tests. The PID gains were manually tuned, resulting in $K_p = 10$, $K_i = 1.5$, and $K_d = 1$ for the releasing phase, while for the reeling phase, a simpler PI controller was sufficient with $K_p = 5$ and $K_i = 0.5$. The mechanical behavior of the tether in both directions was taken into account in the controller tuning approach. Specifically, the tether must be properly wound by the winch while also moving smoothly underwater to avoid disturbing the ROV's maneuverability and the V-shape system.

Subsystem	Parameter	Symbol	Value	Unit
DC Motor	Resistance	R	1.02	Ω
	Inductance	L	5.76×10^{-5}	H
	Rotor inertia	J_m	5.05×10^{-7}	$\mathrm{kg \cdot m^2}$
	Torque constant	k_c	9.18×10^{-3}	$\mathrm{N \cdot m \cdot A^{-1}}$
	Back-EMF constant	k_e	9.18×10^{-3}	$\mathrm{V \cdot s}$
Gearbox	Gear ratio	r_g	1/21	–
	Inertia	J_g	5.01×10^{-8}	$\mathrm{kg \cdot m^2}$
	Efficiency	η_g	0.81	–
Gearwheel	Radius	R_p	25.85×10^{-3}	m
	Mass	m_p	0.075	kg
	Damping coefficient	b_p	–	$\mathrm{N \cdot m/(rad/s)}$

Table 1: Parameters of the tension module

4.2.3. Interbuoy Distance Servoing of the Winch

As the interbuoy distance signal from the V-shape system reflects the need to release or reel-in cable, a dedicated control strategy was implemented (Fig. 8). A PD (Proportional-Derivative) controller was selected for this purpose. The derivative term was introduced to ensure a fast and responsive system behavior, allowing it to react promptly to changes in the V-shape opening and maintain a semi-taut configuration of the tether. The proportional and derivative gains were experimentally tuned and shown to perform well for both reeling and releasing operations using the same values: $K_p = 2.0$ and $K_d = 1.0$. A *Speed Limiter and Safety* module was also developed to ensure operation within the winch's operating range and to prevent excessive cable retraction.

5. Human–Machine Interface

To easily pilot the fully integrated ROV/USV/winch/V-shape system, where data and controllers overlap, a dedicated Human–Machine Interface (HMI) was developed, providing a single point of control and monitoring for all four subsystems. The HMI is implemented as ROS2 nodes (`/hmi/main`) on the operator's PC, communicating with each subsystem's driver node and the joysticks (`/joystick`).

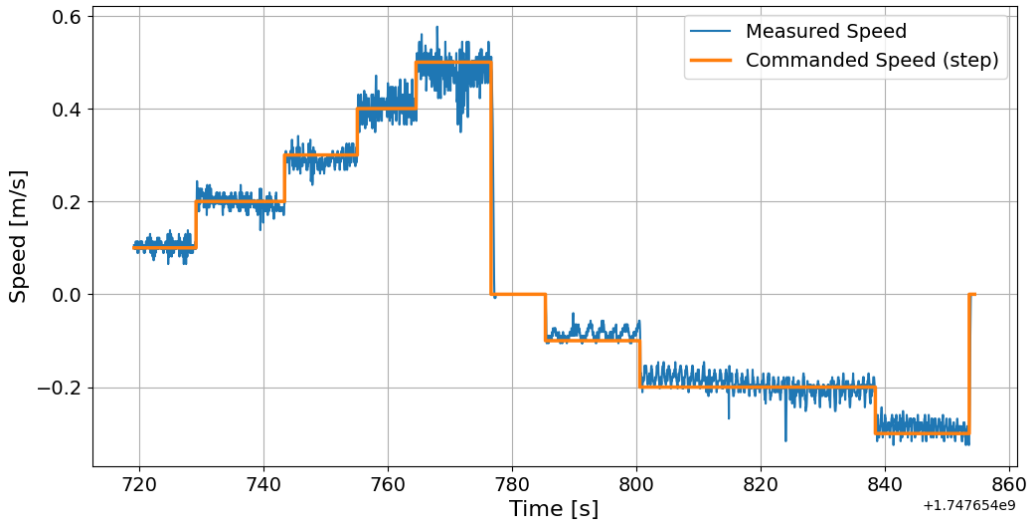

Figure 7: Step responses for commanded speeds of 0.1, 0.2, 0.3, 0.4, 0.5 m/s (releasing) and -0.1, -0.2, -0.3 m/s (reeling-in)

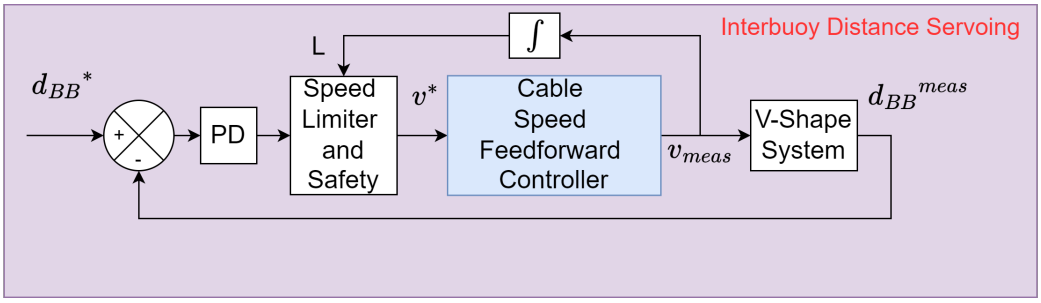

Figure 8: Closed-loop Interbuoy Distance Servoing Diagram for the DC motor of the Tension Module

5.1. ROS Architecture

Fig. 9 shows the simplified ROS 2 architecture. All ROS2 nodes — including `/usv/main`, `/rov/main`, `/v-shape/main`, and `/winch/main` — run on the operator's PC. Raw sensor and actuator data of each subsystem are streamed over UDP or serial to the PC, then rosified into topics by lightweight driver nodes. The central `/hmi/main` node publishes and subscribes to:

- `/usv/...` topics for USV telemetry and commands,
- `/rov/...` topics for ROV telemetry and commands,
- `/v-shape/...` for interbuoy distance and IMU raw data,
- `/winch/...` for cable length, desired and measured linear cable speed and switch states,
- `/joystick/...` for manual override and mode selection.

Additionally, the HMI hosts several processing nodes responsible for key system functionalities. These include sensor fusion, such as applying a Madgwick filter on IMU data to provide yaw correction for both the USV and the ROV, and battery monitoring by converting voltage readings into percentage values for easier interpretation. The HMI also manages dual-joystick assignment and mapping to robot motions, as well as compensation of thruster dead zones to improve control accuracy. Other essential functions handled by the HMI are the conversion of pressure readings into depth estimations, the execution of control laws, including heading hold, depth keeping, surge control, and stabilization modes for both the USV and ROV, and the calibration of the V-shape IMUs along with the estimation of the interbuoy distance. Finally, it provides the interface with the winch, managing both the UDP dispatch of speed commands and the integration of winch data, such as cable length, switch states, and measured speed, into the ROS framework. By centralizing both raw data handling and intermediate processing, the HMI ensures that the GUI layer remains streamlined and responsive.

5.2. Graphical User Interface

Building on this unified backend, the GUI provides the operator with one-click actions, live feedback, and streamlined data capture. The interface (Fig. 10), developed using PyQt5, is organized into five top-level tabs: **Info**, **USV**, **ROV**, **Winch**, and **IMU V-shape**. The **Info** tab provides

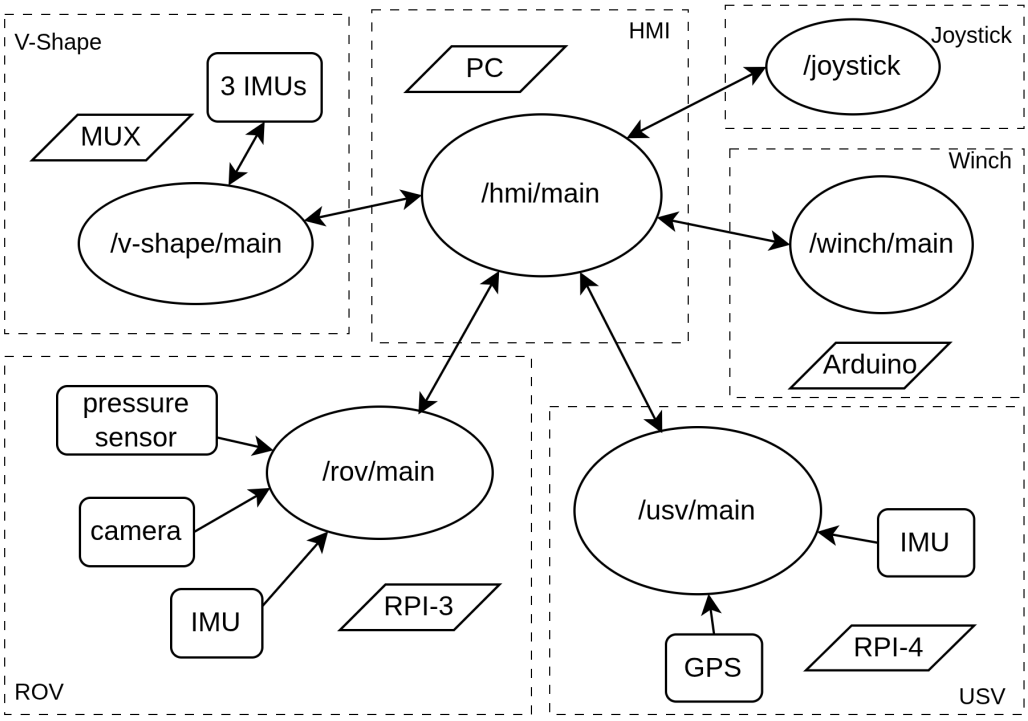

Figure 9: Simplified ROS 2 architecture of the HMI: the central `/hmi/main` nodes communicate with each subsystem nodes (`/usv/main`, `/rov/main`, `/v-shape/main`, `/winch/main`) and the `/joystick` interface.

an overview of the current operating modes of the entire system. It also allows the operator to bind joysticks to the robots, up to two joysticks at the moment, to handle manual control. Additionally, it offers functionalities to arm the robots as part of the safety procedures and to record specific data streams needed for analysis. The **USV** and **ROV** tabs allow the operator to display sensor and actuator data for the corresponding robot. They also provide controls to select the desired operating mode, either manual or one of several predefined autonomous behaviors. Navigation functionalities such as heading hold, stabilization, and depth control can be activated via dedicated checkboxes. Additionally, these tabs include developer-oriented sliders for fine-tuning control parameters, such as PID gains, during experimental phases. As a safety feature, they also allow the operator to shut down or reboot each robot individually via SSH if necessary. The **Winch** tab enables the operator to initiate the connection with the winch and displays all the previously introduced feedback data. It provides checkboxes to select the desired operating mode, either the autonomous interbuoy distance mode or manual control of cable length or speed, with buttons to adjust the setpoint in manual modes. Finally, the **IMU V-shape** tab handles the connection to the V-shape sensor subsystem, involving an SSH connection to the ROV's onboard Raspberry Pi 3B+ to establish I^2C communication with the IMUs. After a 5 s calibration phase, the data stream is transmitted to the PC via UDP. This tab also displays the estimated interbuoy distance along with the connection status.

6. Experiments

6.1. Experimental Setup

The ROV used in this work is the heavy configuration of the BlueROV2[7], equipped with eight T200 thrusters. The USV, on which the winch is mounted, is based on the HyDrone platform[8] and was custom-built by an industrial partner located in Toulon specifically for this project. It is propelled by two T200 thrusters and weighs approximately 15 kg in air, with overall dimensions of 115 cm in length, 75 cm in width, and 55 cm in height. The total mass of the winch is approximately 10 kg, including around 650 g

[7] `https://bluerobotics.com/store/rov/bluerov2-upgrade-kits/brov2-heavy-retrofit/`

[8] `https://www.seafloorsystems.com/hydrone`

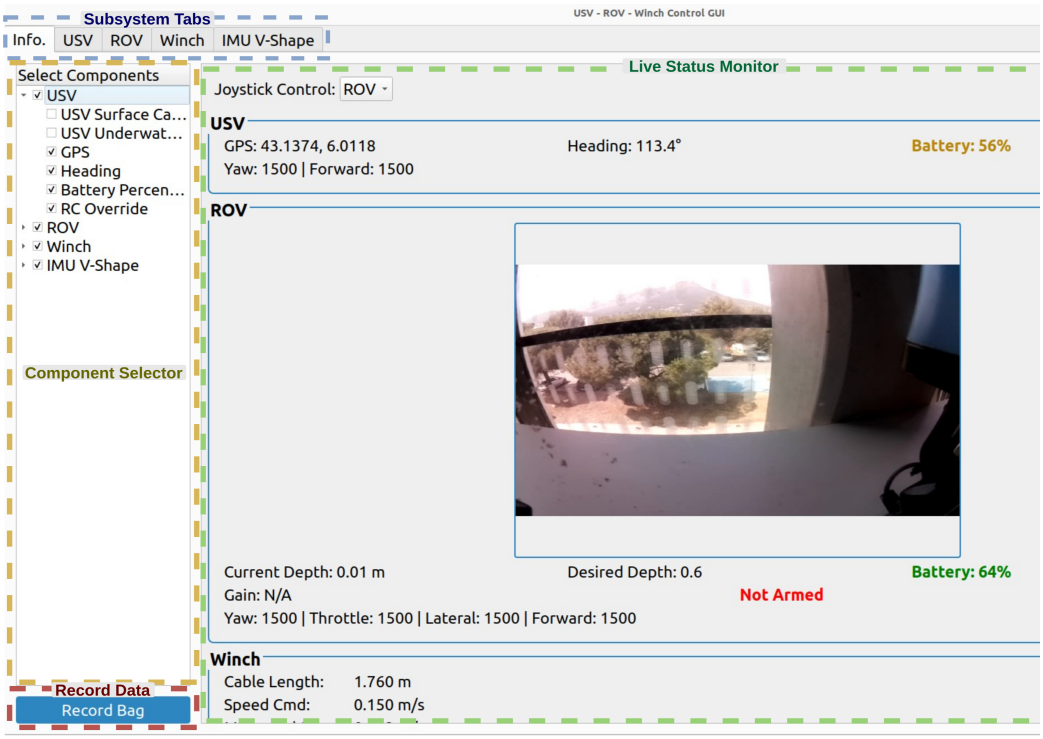

Figure 10: Overview of the GUI: subsystem tabs (blue), live status monitor (green), component selector (yellow), Record Bag button (red).

of wound cable and its onboard battery. The robots are connected by a 50-meter-long Fathom tether composed of a single twisted pair[9]. Communication with the operator is established through a Wi-Fi antenna with a range of 1 km, mounted on the USV, which relays all necessary information to the overall system.

The experiments were conducted in three different environments: a water tank measuring 10 m in length, 3 m in width, and 1.5 m in depth; a rectangular pool measuring 8 m × 4 m with a depth of 2 m; and a circular pool with a diameter of 4 m and a height of 1.25 m. Several cameras were positioned to capture video footage of the tests. All system data, including internal sensor readings and control commands, were recorded using the ROS2 bagging tool integrated into the HMI architecture.

6.2. Assessing Semi-Taut Configuration

6.2.1. V-shape Behavior vs ROV Forward Command

As mentioned in Section 3, the semi-taut cable configuration is useful to minimize drag forces and the risk of entanglement with the environment. This configuration can be determined by analyzing the interbuoy distance data acquired by the V-shape device. However, when the ROV is in motion, viscous drag forces exerted by the surrounding fluid tend to open the V-shape system and to change the natural distance between the buoys. Thus, to release an appropriate length of cable under such conditions, it is necessary to characterize this natural interbuoy distance as a function of the ROV's forward velocity.

To this end, an underwater experimental procedure was conducted in which a significant length of cable was initially deployed while the winch was kept deactivated. As the ROV is not equipped with a linear velocity sensor, its forward control command was used as a proxy for velocity. By applying various forward commands to the ROV and allowing the system to reach steady-state conditions, the corresponding equilibrium interbuoy distance was recorded (Fig. 11). A fifth-degree polynomial was then fitted to the experimental data to serve as a model. To maintain a semi-taut configuration, the targeted interbuoy distance is set to slightly exceed this natural equilibrium value. This experiment thus provides a foundation for

[9] `https://bluerobotics.com/store/cables-connectors/cables/fathom-rov-tether-by-the-meter/`

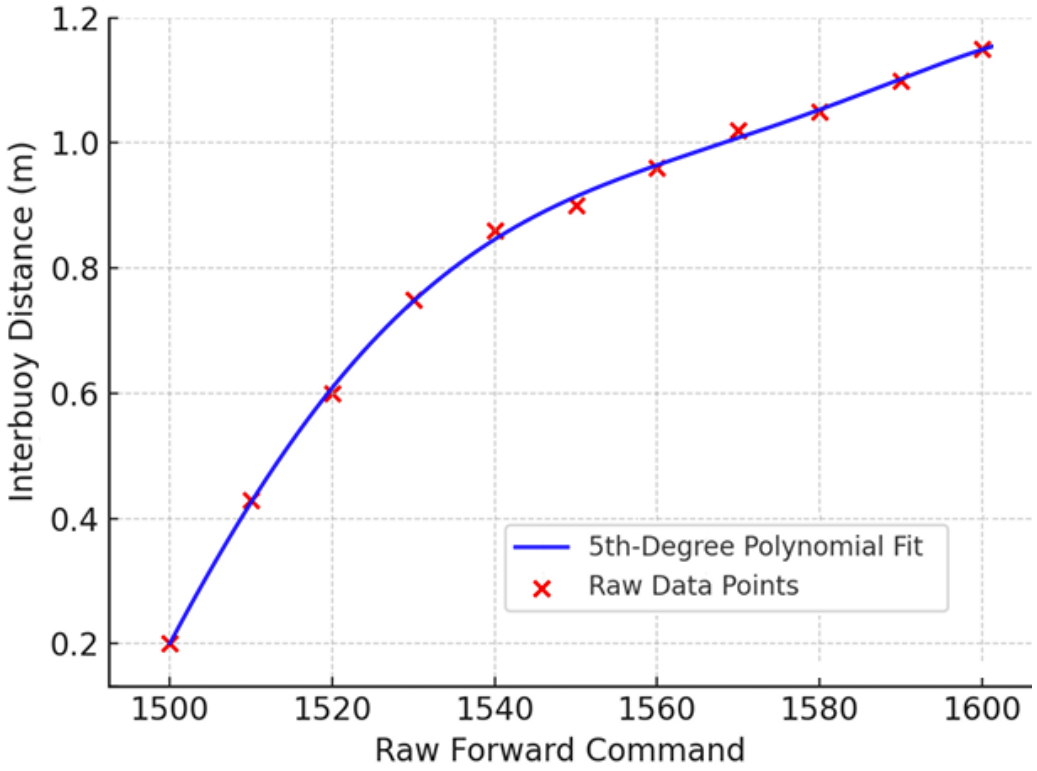

Figure 11: Interbuoy Distance vs ROV Forward Command

adapting the winch control strategy by dynamically adjusting the desired interbuoy distance in response to the ROV's forward command.

6.2.2. Maintaining the Semi-Taut Configuration

To validate the capability of the servo-controlled winch to maintain a semi-taut configuration, several experiments were conducted, involving two representative types of motion : a Round-Trip manoeuver, consisting of sequential forward and backward surge motions, and a C-turn, combining forward surge and yaw motions to produce a C-shaped trajectory. Fig. 12 and Fig. 13 present the results of the Round-Trip and C-turn experiments, respectively, with corresponding video recordings provided in the figure legends. The PD controller gains for the interbuoy distance servoing, as described in section 4.2.3, were determined through experimental tuning. As shown in the videos, the robot is able to move without being disturbed by the tether throughout its trajectory, whether performing straight-line motions or turns.

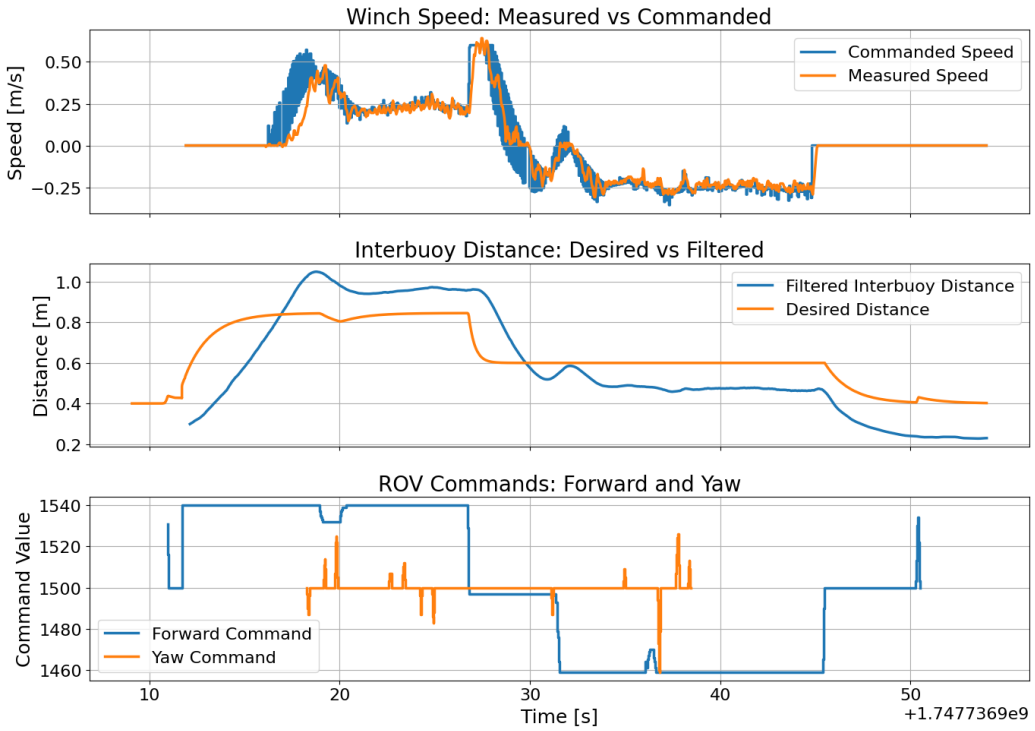

Figure 12: Round-Trip run. Top: winch speed command (blue) vs. measured speed (orange). Middle: desired interbuoy distance (orange) vs. filtered measured distance (blue). Bottom: ROV forward and yaw commands. `https://youtu.be/tfrkL6X7qOo`

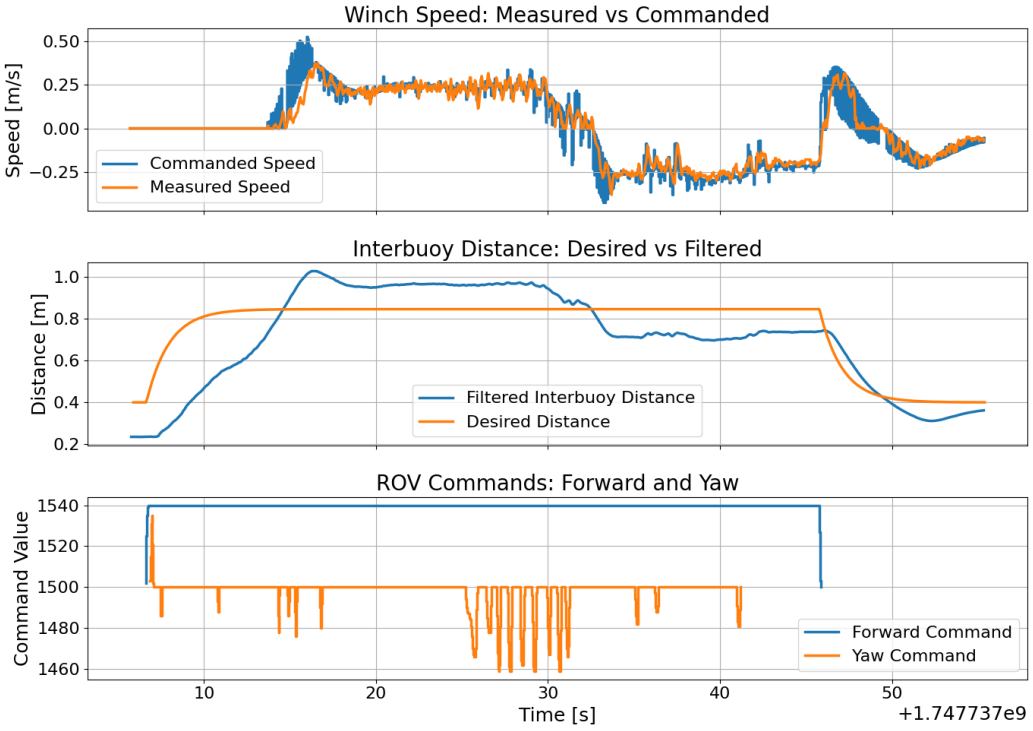

Figure 13: "C–turn" run. Same layout as in Fig. 12. `https://youtu.be/MqwHu8fHHkA`

6.2.3. Knot-Tying Attempt

Previous experiments have shown that the controlled winch effectively maintains a semi-taut cable configuration, thereby minimizing the amount of deployed cable. Consequently, shorter deployed lengths inherently reduce drag forces. An additional experiment was conducted to evaluate the system's ability to mitigate the risk of the cable becoming entangled with itself or the environment. In this test, the ROV was manually piloted with the specific objective of attempting to entangle the cable and form a knot. The USV was left free to drift on the surface. Two trials were carried out: one with winch interbuoy distance control enabled, and one without. For the purpose of the second experiment, a significant length of cable, around 5 m, was deliberately deployed beforehand. Figure 14 shows a video frame of one of the experiments, and the associated videos are provided in the figure caption.

When the winch is not controlled, the ROV may reach configurations that pose risks to the reliability of its mission. Due to its inherent properties, the cable exhibits a natural torsion, which is further accentuated by being stored on a spooler. As a result, a large deployed length tends to accumulate and form a cluster, which can be observed at the beginning of the video. This accumulation leads to several issues, as exhibited in the video. At 0 : 55, the ROV moves away from the cable cluster but is forced to drag the entire mass due to the cable being entangled within it. At 1 : 36, the ROV directly encounters the cable cluster, a situation that could lead to several risks, such as interference with directional acoustic sensors or potential damage to the cable caused by onboard actuators, such as manipulation or sampling tools mounted on the ROV. Finally, at 1 : 56, the ROV becomes entangled in the cable, restricting its movements and causing disturbances on the USV. In most cases, such entanglements cannot be resolved without manual intervention.

Using the interbuoy distance control for the winch effectively mitigates all of these issues. Although the ROV performs random movements, the semi-taut configuration prevents the formation of clusters and knots in the cable. As a result, the ROV is able to operate under favorable conditions around the USV. It is interesting to note that even though the USV is not actuated, it naturally tends to align itself with the direction of the ROV. This behavior is attributed to the semi-taut configuration of the tether, which generates a torque around the USV's vertical axis. However, environmental conditions

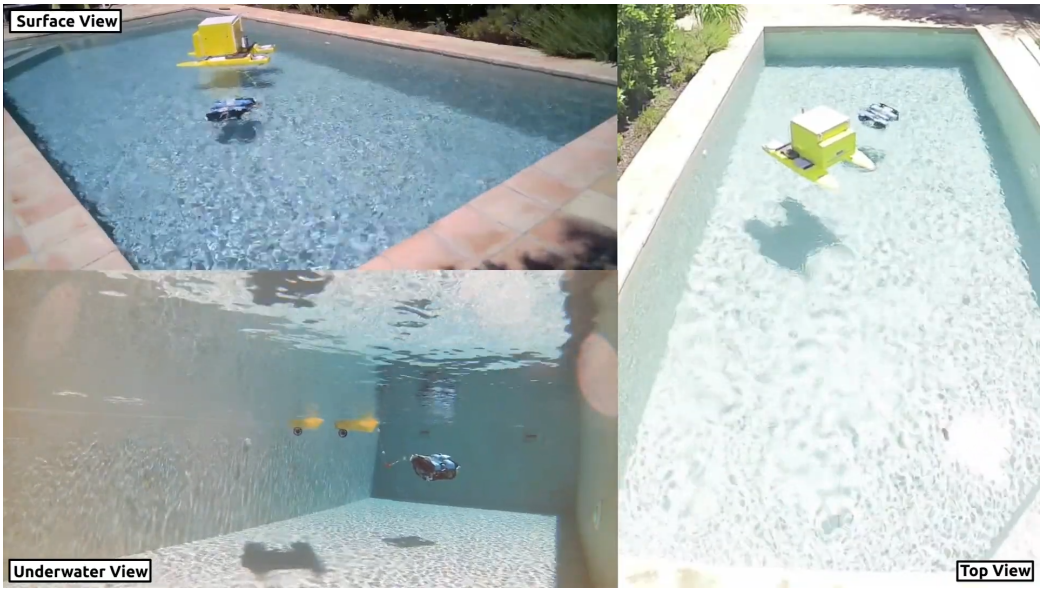

Figure 14: Knot tying attempt experiments. Without controlled winch (`https://youtu.be/H8mcCbAyHhE`), with interbuoy distance controlled winch (`https://youtu.be/7PJ_wkBO8sk`)

during the experiment, such as wind-induced waves and hydrodynamic drag on the USV, may also influence this motion.

6.3. Validation of Heading Alignment

6.3.1. Switch Behavior Validation

As previously mentioned, the winch is equipped with two microswitch sensors on its front panel, which detect whether the cable is departing to right or left side relative to the USV's heading. Their activation relies on the semi-taut configuration maintained by the winch. The more responsive the winch, the more likely it is to induce small jerks in the cable, which can in turn enhance sensor activation and improve the detection of the cable's departure direction. Additionally, during reel-in phases, the pulling force applied to the cable is transmitted along the actuation direction of the switch mechanism, thereby improving detection effectiveness. The vertical inclination of the one switch was also intentionally adjusted to reduce their travel distance and study the impact on the sensitivity.

To estimate the effective detection range of the switches under real operating conditions, a dedicated experiment was conducted in a pool. The ROV

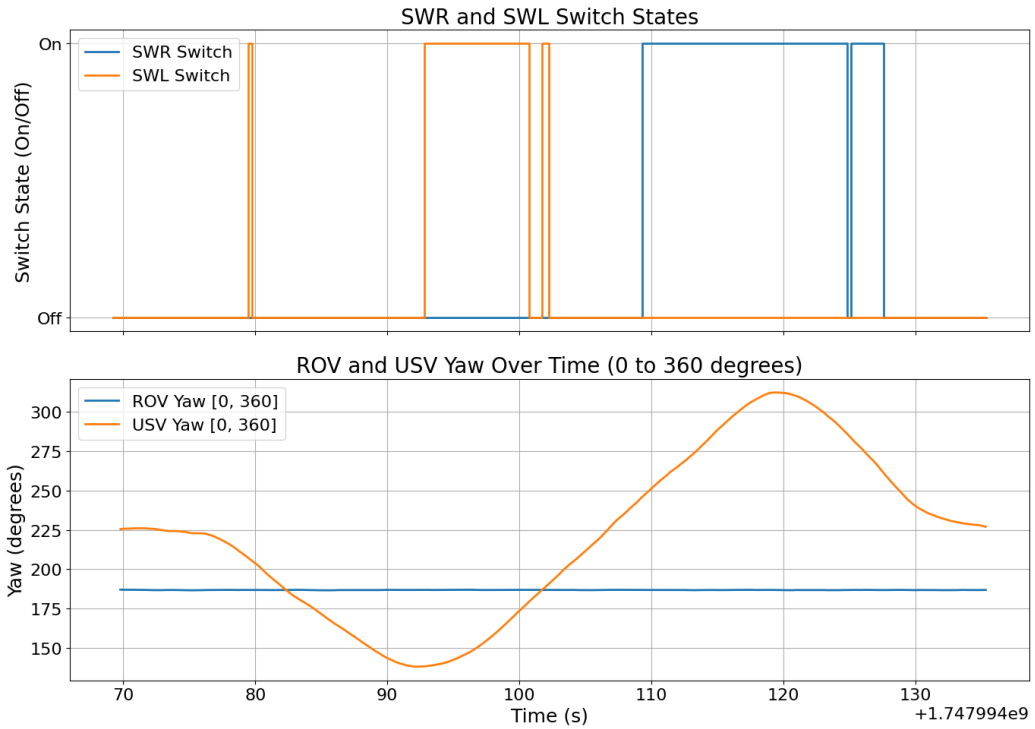

Figure 15: Switches activation and deactivation angles while USV is rotating and ROV still (`https://youtu.be/s564AWdTk6w`).

was fixed at one end of the area, while the USV was positioned several meters away, oriented towards the ROV, with the winch operating in interbuoy distance control mode. By slowly rotating the USV on the spot, first in one direction and then in the other, it was possible to determine the activation and deactivation angles for each switch (Fig. 15). Due to the asymmetric nature of the switch contact mechanism, the activation and deactivation angles differ, as observed during the experiment. Moreover, it was noted that the switch with an initial inclination tends to activate more easily. This experiment demonstrates that the switches are generally capable of correctly indicating deviations of the ROV alignment relative to the USV's axis when operating in semi-taut mode, provided that the system is able to trigger the switches effectively.

In this new experiment, the USV remains still while the ROV moves in front of it, traversing from right to left and vice versa, with the semi-taut mode active. The objective of this experiment is to demonstrate the effec-

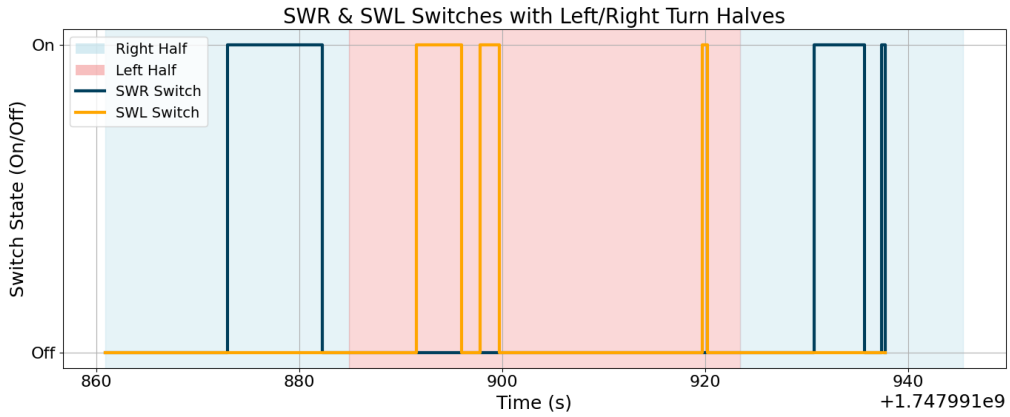

Figure 16: Switches activation and deactivation angles while ROV is rotating around the still USV (`https://youtu.be/xVJTxzvYIrc`).

tiveness of the proposed solution in a more realistic scenario, which appears to be confirmed by the experimental results (Fig. 16). These results show that the right and left switches successfully detect the presence of the ROV within the appropriate regions.

6.3.2. Heading Alignment

This final experiment builds upon the results of the experiments presented in section 6.2.3 and section 6.3.1. It was previously observed that maintaining a semi-taut cable configuration tends to passively align the unactuated USV in the direction of the ROV. However, since this rotation is not actively controlled, it cannot be considered reliable. Nonetheless, the switches installed on the winch appear to be capable of indicating whether the ROV is moving outside a certain angular range relative to the USV's heading. By combining these two approaches, a dedicated heading control algorithm for the USV was developed. When a switch is activated, the USV initiates a slow rotation to bring the switch back to its deactivation point. Once this point is reached, the USV continues to rotate to position itself at the center of the known switch's angular detection range. The semi-taut cable configuration allows the ROV to move freely while also enhancing switch activation, making this strategy suitable for enabling angular tracking of the ROV by the USV.

In this experiment, the ROV was initially positioned in front of the USV

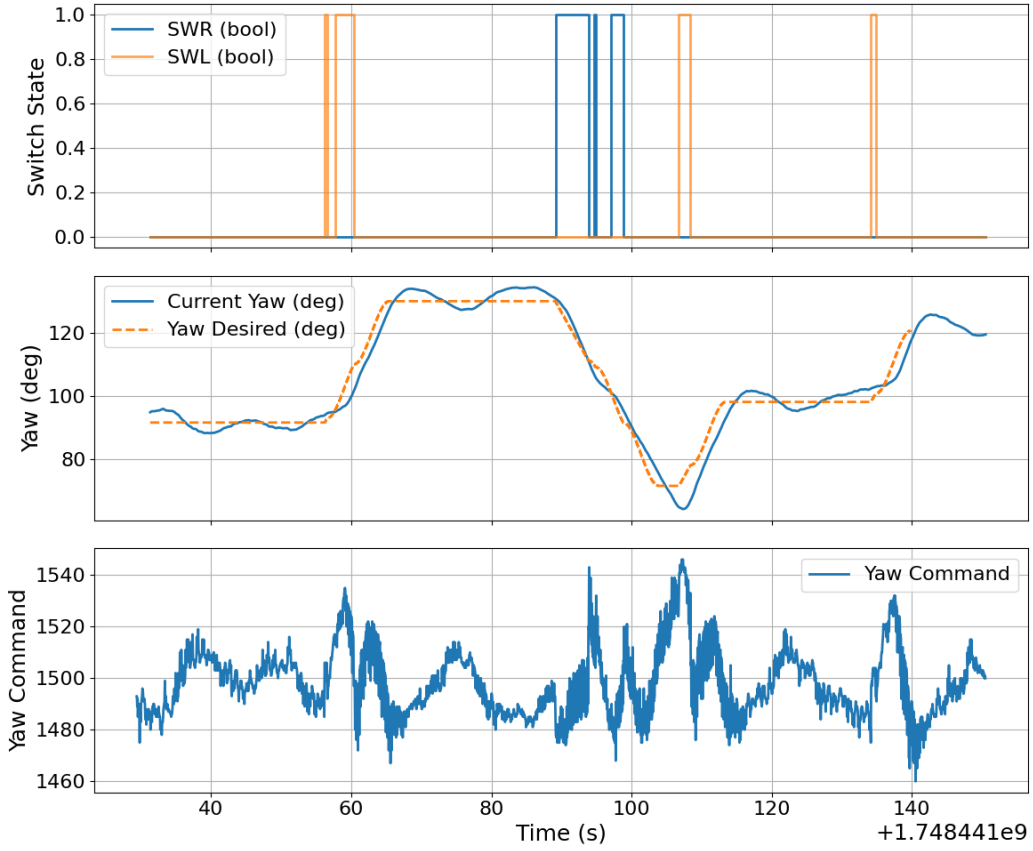

Figure 17: Switch-based heading alignment data (three subplots). Top: SWR (blue) and SWL (orange) boolean states (1 = on, 0 = off). Middle: Desired yaw (dashed orange) vs. USV yaw (solid blue). Bottom: Yaw-thruster command sent to the USV. (`https://youtu.be/LoNDW-X1hmI`)

and then commanded to move laterally to the left until the left switch (SWL) was triggered. Once activated, the USV adjusted its yaw using the previously introduced algorithm to realign with the ROV, and then the opposite scenario was tested using the right switch (SWR). The slow yaw rotation value used for this experiment was $4\,^{\circ}/\mathrm{s}$. The results are presented in Fig. 17, with the associated video provided in the figure caption. As observed, the USV is controlled to align with the ROV, although the control gains could be further tuned to meet specific behavioral requirements, if necessary.

All these experiments demonstrate that each component of our mechatronic solution works correctly. The new IMU-based V-shape device can now

detect and evaluate the need to release or reel in the tether in any ROV configuration. The winch, driven by feedback signals, continuously adjusts the tether length. The spooler winds the tether smoothly, preventing entanglement of the coiled tether without interfering with the tension module. Switch sensors placed at the winch inlet reliably indicate the direction of tether movement, and thus the direction of the ROV relative to the USV heading, provided that water disturbances (e.g., large waves or strong currents) are not excessive. Altogether, these combined functions pave the way for autonomous collaboration between the USV and ROV systems.

7. Conclusion

This work aims to upgrade ROV/USV systems to make them more cable-aware, thereby eliminating risky configurations such as tether entanglement with obstacles or self-interference, which can degrade ROV maneuverability or lead to mission-critical failures. To achieve this, a two-part solution was developed. A compliant IMU-Based V-shape solution, positioned on the tether just aft of the ROV, passively reduces the forces exerted on the robot and enables estimation of the required tether length. In parallel, an intelligent winch installed on the USV meets this demand by automatically adjusting the cable length, maintaining a so-called "semi-taut configuration," which also aids in detecting the ROV's orientation relative to the USV's heading. Experimental validation demonstrates that this solution allows the ROV to operate freely, with the USV autonomously managing tether delivery and sensing the ROV's direction.

The prospects of this work are manifold, as they open the way for autonomous following of the ROV by the USV, adapted to various mission objectives. For this purpose, control strategies based on tether's configuration and directional feedback can be developed to enhance coordination between surface and underwater vehicles. Additionally, this approach provides a foundation for further investigation into relative underwater localization, a key challenge in cooperative marine robotics. Ongoing developments in this direction are expected to be the subject of future scientific publications.

References

[1] R. Capocci, G. Dooly, E. Omerdić, J. Coleman, T. Newe, D. Toal, Inspection-Class Remotely Operated Vehicles—A Review, Journal of

Marine Science and Engineering 5 (1) (2017) 13. doi:10.3390/jmse5010013.
URL http://www.mdpi.com/2077-1312/5/1/13

[2] M. Ludvigsen, A. J. Sørensen, Towards integrated autonomous underwater operations for ocean mapping and monitoring, Annual Reviews in Control 42 (2016) 145–157. doi:10.1016/j.arcontrol.2016.09.013.
URL https://www.sciencedirect.com/science/article/pii/S1367578816300256

[3] A. Ghatak, K. Mukherjee, Y. Singh, Classification on unmanned underwater vehicles: a review, International Journal of Vehicle Autonomous Systems 1 (01 2024). doi:10.1504/IJVAS.2024.10064856.

[4] A. Merci, C. Anthierens, N. Thirion-Moreau, Y. Le Page, A simulator of underwater glider missions for path planning, Ocean Engineering 269 (2023) 113514. doi:10.1016/j.oceaneng.2022.113514.
URL https://linkinghub.elsevier.com/retrieve/pii/S0029801822027974

[5] H. Cho, S.-K. Jeong, D.-H. Ji, N.-H. Tran, M. T. Vu, H.-S. Choi, Study on control system of integrated unmanned surface vehicle and underwater vehicle, Sensors 20 (9) (2020). doi:10.3390/s20092633.
URL https://www.mdpi.com/1424-8220/20/9/2633

[6] G. Conte, D. Scaradozzi, D. Mannocchi, P. Raspa, L. Panebianco, L. Screpanti, Development and Experimental Tests of a ROS Multiagent Structure for Autonomous Surface Vehicles, Journal of Intelligent & Robotic Systems 92 (3-4) (2018) 705–718. doi:10.1007/s10846-017-0700-9.
URL http://link.springer.com/10.1007/s10846-017-0700-9

[7] N. Kapetanović, K. Krčmar, N. Miskovic, Nađ, Tether Management System for Autonomous Inspection Missions in Mariculture Using an ASV and an ROV, IFAC-PapersOnLine 55 (2022) 327–332. doi:10.1016/j.ifacol.2022.10.450.

[8] M. T. Vu, M. Van, D. H. P. Bui, Q. T. Do, T.-T. Huynh, S.-D. Lee, H.-S. Choi, Study on Dynamic Behavior of Unmanned Surface Vehicle-Linked Unmanned Underwater Vehicle System for Underwater Explo-

ration, Sensors 20 (5) (2020) 1329. doi:10.3390/s20051329.
URL https://www.mdpi.com/1424-8220/20/5/1329

[9] J. V. Grindheim, Underwater cable dynamics for beginners, in: 29th International Congress on Waterborne Transportation, Shipbuilding and Offshore Constructions, Galoa, 2022. doi:10.17648/sobena-2022-154073.
URL https://proceedings.science/proceedings/100293/_papers/154073

[10] J. Drupt, C. Dune, A. I. Comport, S. Sellier, V. Hugel, Inertial-Measurement-Based Catenary Shape Estimation of Underwater Cables for Tethered Robots, in: 2022 IEEE/RSJ International Conference on Intelligent Robots and Systems (IROS), 2022.
URL https://hal.science/hal-03841236

[11] C. Peraud, M. Filliung, C. Anthierens, C. Dune, N. Boizot, V. Hugel, IMU-based Monitoring of Buoy-Ballast System through Cable Dynamics Simulation, 2024 IEEE/RSJ International Conference on Intelligent Robots and Systems (IROS) (2024). doi:10.1109/IROS58592.2024.10802858.

[12] C. Zhao, P. Thies, L. Johanning, J. Cowles, Modelling and assessment of ROV capacity within an autonomous offshore intervention system, 2020, pp. 755–759. doi:10.1201/9781003134572-86.

[13] C. Zhao, P. Thies, J. Lars, J. Cowles, Rov launch and recovery from an unmanned autonomous surface vessel – hydrodynamic modelling and system integration, Ocean Engineering 232 (2021) 109019. doi:https://doi.org/10.1016/j.oceaneng.2021.109019.
URL https://www.sciencedirect.com/science/article/pii/S0029801821004546

[14] Y. Gu, J. Ni, Z. Geng, B. Zhao, H. Yang, Buoy and winch collaborative control system based on deep reinforcement learning, Journal of Marine Science and Engineering 13 (2) (2025). doi:10.3390/jmse13020326.
URL https://www.mdpi.com/2077-1312/13/2/326

[15] T. Moh, N. Jang, S. Jang, J. Cho, Application of a winch-type towed acoustic sensor to a wave-powered unmanned surface vehicle, Defence Science Journal 67 (2016) 125. doi:10.14429/dsj.67.10577.

[16] R. Bye, O. Osen, W. Rekdalsbakken, B. Skogeng Pedersen, I. Hameed, An intelligent winch prototyping tool, 2017, pp. 276–284. doi:10.7148/2017-0276.

[17] O. Tortorici, C. Anthierens, V. Hugel, A New Flex-Sensor-Based Umbilical-Length Management System for Underwater Robots, in: 2023 European Conference on Mobile Robots (ECMR), IEEE, Coimbra, Portugal, 2023, pp. 1–6. doi:10.1109/ECMR59166.2023.10256299.
URL https://ieeexplore.ieee.org/document/10256299/

[18] O. Tortorici, C. Péraud, C. Anthierens, V. Hugel, Automated Deployment of an Underwater Tether Equipped with a Compliant Buoy–Ballast System for Remotely Operated Vehicle Intervention, Journal of Marine Science and Engineering 12 (2) (2024) 279. doi:10.3390/jmse12020279.
URL https://www.mdpi.com/2077-1312/12/2/279